JOURNAL OF COMPUTATIONAL PHYSICS **126,** 165–180 (1996)
ARTICLE NO. 0128

An Analysis of 1-D Smoothed Particle Hydrodynamics Kernels

DAVID A. FULK AND DENNIS W. QUINN

Department of Mathematics and Statistics, Air Force Institute of Technology, Wright-Patterson AFB, Ohio 45433-7765

Received February 9, 1995; revised September 7, 1995

In this paper, the smoothed particle hydrodynamics (SPH) kernel is analyzed, resulting in measures of merit for one-dimensional SPH. Various methods of obtaining an objective measure of the quality and accuracy of the SPH kernel are addressed. Since the kernel is the key element in the SPH methodology, this should be of primary concern to any user of SPH. The results of this work are two measures of merit, one for smooth data and one near shocks. The measure of merit for smooth data is shown to be quite accurate and a useful delineator of better and poorer kernels. The measure of merit for non-smooth data is not quite as accurate, but results indicate the kernel is much less important for these types of problems. In addition to the theory, 20 kernels are analyzed using the measure of merit demonstrating the general usefulness of the measure of merit and the individual kernels. In general, it was decided that bell-shaped kernels perform better than other shapes.

1. INTRODUCTION

In this paper we analyze the key element in the smoothed particle hydrodynamics (SPH) method, the SPH kernel. The overall goals are twofold. First, to propose and develop a measure of merit for evaluating kernels in one dimensional SPH. Second, to apply this measure to 20 different kernels (several of which are proposed here for the first time) providing an insight into the use of these kernels in SPH.

The numerical technique known as (SPH) is a gridless, pure Lagrangian method for solving the Euler equations of gas dynamics. The basic form of the SPH derivative equation in one dimension is

$$f'(x_i) \approx \sum_{j=1}^{N} \frac{m_j}{\rho_j} f(x_j) W'(x_i - x_j, h), \tag{1}$$

where x is the particle position, m is the mass, ρ is the density, h is the smoothing length of the SPH kernel, and W is the kernel (weighting or smoothing function). The subscripts identify the particle and the derivative on the kernel is with respect to x_i. The kernel is assumed to have compact support, so the sum is over only neighboring particles. Some background in SPH is assumed in this paper. Readers are referred to a recent overview by Monaghan [1] or to work by Fulk [2] or Fulk and Quinn [3]. For recent applications of SPH see Monaghan [4] or Libersky *et al.* [5].

To some extent it should not matter what kernel is used in SPH as long as basic requirements are met. This is especially true in the limit as h (the kernel smoothing length) and Δx (the interparticle spacing) become small. But when they are not small, as is common in practice, the choice of kernel can drastically change the computational results. Hence, the choice of kernel is a key decision before performing any calculation using SPH. This paper provides an objective means of separating better from poorer kernels. The properties we require for an SPH kernel in this paper are that it is even, normalized, and has compact support.

In performing the analysis we also consider 20 SPH kernels. Some of them were obtained from the published literature for SPH (such as Wood [6] and Monaghan [7]) and unpublished literature (such as Morris [8]). But, most of the kernels were created for this analysis. The kernels can be divided into four categories based on the general shape of the kernel: bell shaped, parabolic shaped, hyperbolic shaped, or double hump. A sample for each of these kernel shapes and its derivatives is shown in Fig. 1. The bell shaped kernels resemble a normal or Gaussian curve. The parabolic shaped kernels resemble a downward opening parabola. The hyperbolic shaped kernels resemble the negative exponential function (a hyperbolic function). The double hump kernels are bell kernels that were modified to have two local maxima.

The 20 kernels considered in this paper are shown in Table I. In the table, the "Type" column is either: B—bell shaped; P—parabolic shaped; H—hyperbolic shaped; or D—double hump shaped. Also in the table, "c_n" is the normalization constant for one dimension (1D). These kernels all meet the minimum requirements for an SPH kernel and are of the form $W(x, h) = (1/h)K(x/h) = (c_n/h)\mathcal{K}(x/h)$, where c_n is the normalization constant. Consequently, the functions $K(u)$ and $\mathcal{K}(u)$ are the same, except that $K(u)$ is normalized and $\mathcal{K}(u)$ is not. Note: $\mathcal{K}(u)$ is shown in Table I. These kernels are also all defined to be zero for $|u| > 2$. Additional kernels with support (κ) greater than 2 are discussed in Section 4.

0021-9991/96 $18.00

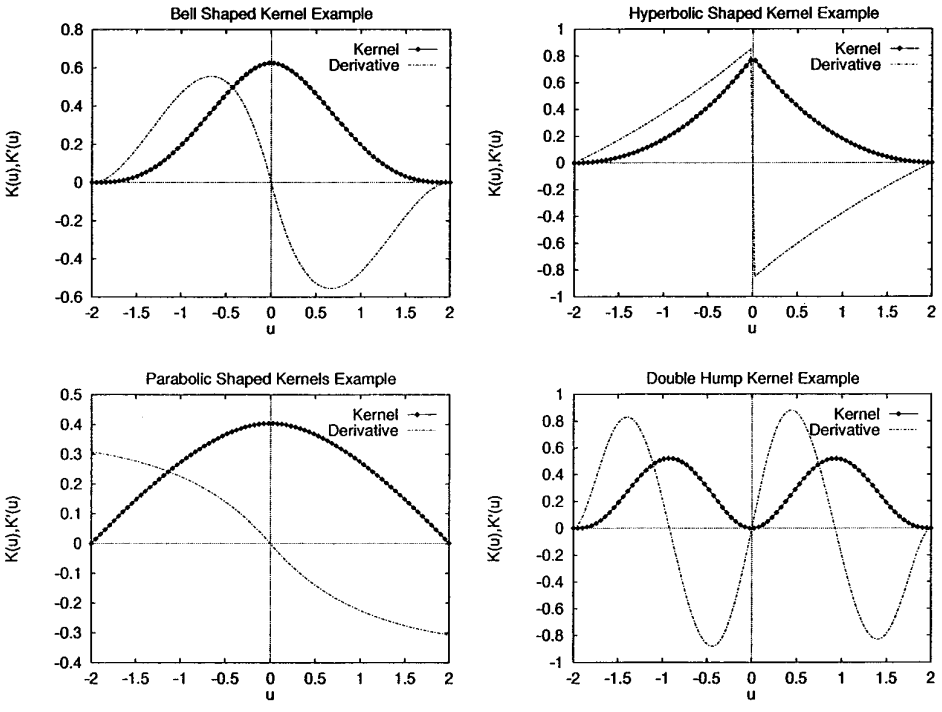

FIG. 1. General shapes of kernels studied.

This paper contains four parts. In Section 2 a measure of merit from the error arising in consistency analysis is developed. In Section 3 a measure of merit based on lower order polynomials under uniform space conditions is proposed and developed. In Section 4 work similar to Sections 2 and 3 is performed for kernels with larger compact support and so-called higher order kernels. In Section 5 a measure of merit for kernels near a discontinuity is proposed and developed.

2. ACCURACY FROM CONSISTENCY ANALYSIS

As shown in Fulk [2] or Fulk and Quinn [3], SPH is developed in a two-step approach. The first step, known as the kernel approximation, uses the Taylor series expansion

$$f'(x) = f'(x_i) + (x - x_i)f''(x_i) + \frac{(x - x_i)^2}{2} f'''(\xi(x, x_i))$$

to obtain

$$f'(x_i) = \int_\Omega f'(x)W(x_i - x, h)\, dx + E_k(f, x_i), \qquad (2)$$

where the error term

$$E_k(f, x_i) = \frac{1}{2}\int_\Omega u^2 W(-u, h) f'''(\xi_i(u))\, du \qquad (3)$$

is obtained from the Taylor remainder term. Note the second derivative term vanishes because the kernel is even. The Taylor series produces a remainder $f'''(\xi)$ which depends on the variable of integration and x_i; hence we use the function $\xi_i(u) \in \Omega$ in the error term. The second step, known as the particle approximation, can be arrived at from several points of view. Regardless, it must be some form of a quadrature rule. We elected to use a composite rectangular rule argument in Fulk [2] or Fulk and Quinn [3],

$$\sum_{j=1}^{N} \int_{x_j}^{x_{j+1}} F(x)\, dx = \sum_{j=1}^{N} \left[(x_{j+1} - x_j)F(x_j) + \frac{1}{2}(x_{j+1} - x_j)^2 F(\xi_j) \right].$$

This obtains

$$f'(x_i) = \sum_{j=1}^{N} \Delta x_j f(x_j) W'(x_i - x_j, h) + E_r(f, x_i) + E_k(f, x_i), \qquad (4)$$

where the error term from the second step is

$$E_r(f, x_i) = \frac{1}{2}\sum_{j=1}^{N} \left[\frac{(x_{j+1} - x_j)^2 + (x_j - x_{j-1})^2}{2} \right] \qquad (5)$$

TABLE I

One-Dimensional Kernels Analyzed

No.	Name	Type	$\mathscr{K}(u)$	1D c_n
1	W_4 B-spline	B	$1-\frac{3}{2}u^2+\frac{3}{4}\lvert u\rvert^3$ if $0\le\lvert u\rvert\le 1$; $\frac{1}{4}(2-\lvert u\rvert)^3$ if $1\le\lvert u\rvert\le 2$	$\frac{2}{3}$
2	Cosine	B	$\left(1-\frac{u^2}{4}\right)\left(1+\cos\left(\frac{\pi u}{2}\right)\right)$	$\frac{3\pi^2}{8(\pi^2+3)}$
3	$\kappa-2$ Gaussian	B	$e^{-2.25u^2}-e^{-9}$	0.846657
4	L Gaussian	B	$(2-\lvert u\rvert)e^{-u^2}$	0.392674
5	Q Gaussian	B	$\left(1-\frac{u^2}{4}\right)e^{-u^2}$	0.643998
6	T Gaussian	B	$e^{-u^2}-e^{-4}$	0.591401
7	Quartic-1	B	$(2+3\lvert u\rvert)(2-\lvert u\rvert)^3$	0.0390625
8	Quartic-2	B	$16-8\lvert u\rvert^3+3u^4$	0.0260417
9	$\kappa-2$ Exponential	H	$e^{-4.5\lvert u\rvert}-e^{-9}$	2.250555
10	1/X,2	H	$\frac{1}{2+\lvert u\rvert}+\frac{\lvert u\rvert-6}{16}$	7.337061
11	1/X,4	H	$\frac{1}{4+\lvert u\rvert}+\frac{\lvert u\rvert-8}{36}$	30.163694
12	1/X,10	H	$\frac{1}{10+\lvert u\rvert}+\frac{\lvert u\rvert-14}{144}$	283.12551
13	$-X^2$	H	$\frac{1}{2}(\lvert u\rvert-2)^2$	0.375
14	$-x-e^{-x}$	P	$2-\lvert u\rvert-e^{-\lvert u\rvert}+e^{-2}$	0.355617
15	$4-X^2$	P	$4-u^2$	0.09375
16	$8-X^3$	P	$8-\lvert u\rvert^3$	0.041667
17	Double B-spline	D	$u^2-\frac{3}{2}u^4+\frac{3}{4}\lvert u\rvert^5$ if $0\le\lvert u\rvert\le 1$; $\frac{1}{4}u^2(2-\lvert u\rvert)^3$ if $1\le\lvert u\rvert\le 2$	2.0
18	Double Q Gauss	D	$u^2\left(1-\frac{u^2}{4}\right)e^{-u^2}$	1.769794
19	Double T Gauss	D	$u^2(e^{-u^2}-e^{-4})$	1.337315
20	Double Q-1	D	$u^2(2+3\lvert u\rvert)(2-\lvert u\rvert)^3$	0.102539

$$[f(\zeta_j)W'(x_i-\zeta_j,h)]'.$$

The variable ζ_j is a point in the interval that is specified by the error analysis. Note: most of this paper assumes a uniform spacing of points, which would actually make the error more like a trapezoid rule. However, we have kept the lower order error term here to be compatible with the background papers and the order of the E_k term. The notation Δx in Eq. (4) is used instead of the more standard SPH use of m/ρ shown in Eq. (1). This is a notational convenience and for uniform spacing (assumed later) the interparticle spacing and field volume in 1D should be the same.

The first thought for a measure of merit is to consider bounds on the error terms derived in the consistency analysis. From Eq. (3), for a sufficiently smooth function, $f(x)$, the $E_k(f, x_i)$ term can be bounded by

$$\max_{\xi\in\Omega}\frac{|f'''(\xi)|}{2}\int_0^\kappa u^2K(u)\,du. \tag{6}$$

When comparing different kernels, the function f will have the same value in Eq. (6), so we only need to use the integral to differentiate between the kernels. For any given kernel function, a lower value from the integral should indicate a better kernel approximation. It would be desirable if this implied that the final SPH approximation is also better for lower values of the integral. Unfortunately, this is not always true. The values for the integral for the 20 kernels are shown in Table II.

The data in this table indicate that the hyperbolic shaped (H) and bell shaped (B) kernels are, for the most part, the better ones and the parabolic shaped (P) and double hump (D) are poorer. However, there are some exceptions. Based on work shown later in this paper, this result holds

TABLE II

Kernel Integral Analysis

No.	Name	Type	$\int_0^K u^2K(u)\,du$
1	W_4 B-spline	B	0.16667
2	Cosine	B	0.206123
3	$\kappa - 2$ Gaussian	B	0.110833
4	L Gaussian	B	0.153629
5	Q Gaussian	B	0.181942
6	T Gaussian	B	0.221115
7	Quartic-1	B	0.190476
8	Quartic-2	B	0.31746
9	$\kappa - 2$ Exponential	H	0.0483464
10	1/X,2	H	0.165735
11	1/X,4	H	0.179783
12	1/X,10	H	0.190883
13	$-X^2$	H	0.2
14	$-x - e^{-x}$	P	0.372537
15	$4 - X^2$	P	0.4
16	$8 - X^3$	P	0.44444
17	Double B-spline	D	0.45
18	Double Q Gauss	D	0.501864
19	Double T Gauss	D	0.59324
20	Double Q-1	D	0.5

only in a limited sense. The reason this indicator does not work as well as desired is because it is evaluating only part of the SPH process, the kernel approximation. It says nothing about the particle approximation and its error $E_r(f, x_i)$. Also, it is a measure of the central peakness of the kernel. That is, the smaller the value, the larger the peak is at 0. If the error from the particle approximation is quite small (as in the case when $\Delta x/h \ll h < 1$), then this indicator would appear more correct. Hence, as $\Delta x/h \to 0$, the integral results would determine the better kernels to use. But for more sparsely spaced particles, which occurs in practice, a smaller value of the integral could quite easily indicate that not enough smoothing is being done because the kernel is too peaked. So at best, the integral results are only one overall indicator of the quality of a kernel.

It would be desirable then to add a term from the error term given in Eq. (5). However, we see that this equation does not allow us to easily remove the function f or its derivative from the analysis. This would seem to apply that the function being evaluated can affect the accuracy as well as the kernel. Hence, this error term is not analyzed further here, but specific cases are considered in the next section.

3. UNIFORM SPACE, SMOOTH DATA ANALYSIS

In this section, functions that are fairly smooth (i.e., no shocks present) are considered and the particles are required to be uniformly spaced. The result is an equation that will form the foundation of a measure of merit for SPH kernels. Start by defining the following:

$$f_i' \approx \sum_{j=1}^{N} \Delta x_j f_j W_{ij}'$$

$$x_i = a + i\,\Delta x_i, \quad \Delta x_i = \Delta x$$

$$x_{ij} = x_i - x_j = a + i\,\Delta x - a - j\,\Delta x = (i-j)\,\Delta x$$

$$W_{ij}' = \frac{1}{h^2} K'\left(\frac{x_{ij}}{h}\right) = \frac{1}{h^2} K'\left((i-j)\frac{\Delta x}{h}\right) = \frac{1}{h^2} K_{ij}'.$$

Note that we are using Δx instead of the more standard m/ρ for the SPH approximation. Although this is a restriction, under the assumptions of this section, it should not affect the results. Now consider particle $i \in (1, N)$ such that $x_i - x_1 > \kappa h$ and $x_N - x_i > \kappa h$. Then examine functions that are constant, linear, and quadratic under the assumptions here to find a basic relationship.

(a) Assume f is constant: $f = c \Rightarrow f' = 0$. Since K is symmetric (even), K' is odd. This then yields

$$0 \approx \sum_{j=1}^{N} \Delta x_j f_j W_{ij}' = \frac{c\,\Delta x}{h^2} \sum_{j=1}^{N} K'\left((i-j)\frac{\Delta x}{h}\right) = \frac{c\,\Delta x}{h^2} K'(0). \tag{7}$$

Therefore, $K'(0)$ must equal zero to model the derivative of a constant function exactly (under the above assumptions on K).

(b) Assume f is linear: $f = cx \Rightarrow f' = c$. Also assume that $K'(0)$ is zero, so that a constant function is exact and $\sum_{j=1}^{N} K_{ij}' = 0$. Expand $f(x_j)$ in a Taylor series about x_i to obtain

$$c \approx \sum_{j=1}^{N} \Delta x_j f_j W_{ij}' = \sum_{j=1}^{N} \Delta x_j (f_i - x_{ij} f_i') W_{ij}'$$

$$= \frac{\Delta x}{h^2} \sum_{j=1}^{N} c(x_i - x_{ij}) K'\left((i-j)\frac{\Delta x}{h}\right)$$

$$= \frac{c x_i\,\Delta x}{h^2} \sum_{j=1}^{N} K_{ij}' - \frac{c\,\Delta x}{h^2} \sum_{j=1}^{N} x_{ij} K_{ij}'$$

$$= c\left[\frac{\Delta x}{h^2} \sum_{j=1}^{N} (x_j - x_i) K_{ij}'\right] = c\left[\frac{\Delta x}{h^2} \sum_{j=1}^{N} (j-i)\,\Delta x\, K_{ij}'\right].$$

Therefore this results in

$$1 \approx \sum_{j=1}^{N} (j-i)\left(\frac{\Delta x}{h}\right)^2 K'\left((i-j)\frac{\Delta x}{h}\right) = -2\sum_{l=1}^{\infty} l\left(\frac{\Delta x}{h}\right)^2 K'\left(l\frac{\Delta x}{h}\right). \tag{8}$$

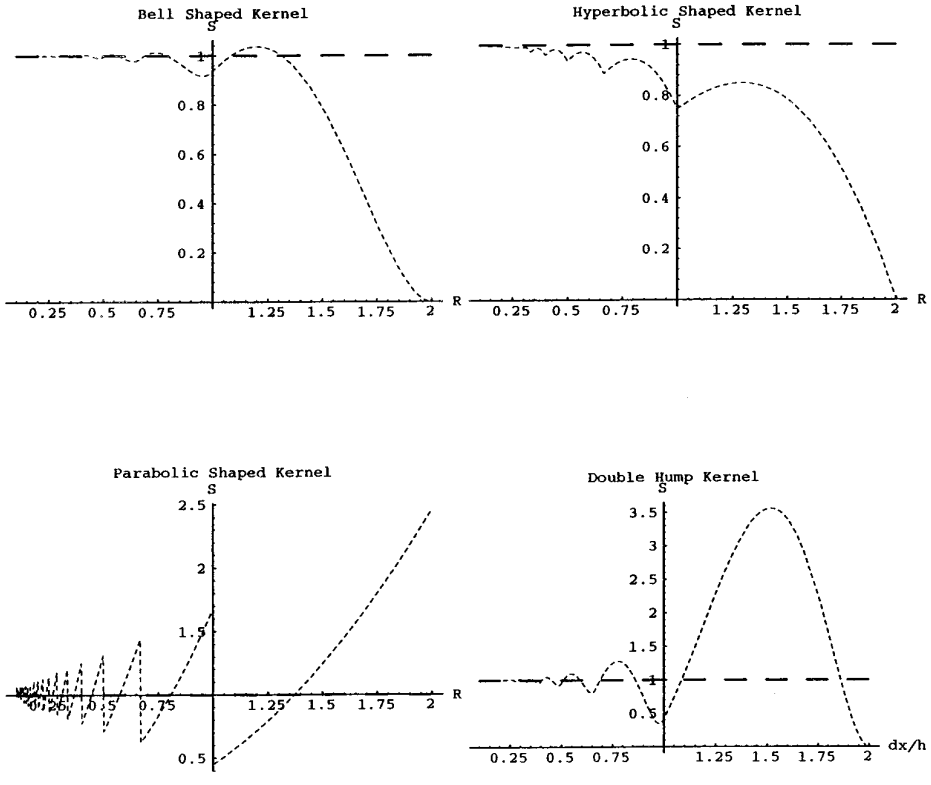

FIG. 2. Result 1 plots.

The last sum is obtained by taking $l = i - j$ and noting that the compact support allows us to sum to ∞, $K'(u)$ is odd so $-uK'(u)$ is even, and $K'(0) = 0$ so only positive indices are used. It is fairly easy to see that no function satisfies Eq. (8) for all values of $\Delta x/h$.

(c) Assume f is quadratic: $f = cx^2 + dx + e \Rightarrow f' = 2cx + d$. Also assume that $K'(0)$ is again zero. As in part (b), expand $f(x_j)$ in a Taylor series about x_i to obtain

$$2cx_i + d \approx \sum_{j=1}^{N} \Delta x_j (cx_i^2 + dx_i + e + 2cx_i x_{ji} + dx_{ji} + cx_{ji}^2) W'_{ij}$$

$$= \frac{(cx_i^2 + dx_i + e)\,\Delta x}{h^2} \sum_{j=1}^{N} K'_{ij} + \frac{c\,\Delta x}{h^2} \sum_{j=1}^{N} x_{ij}^2 K'_{ij}$$

$$- \frac{(2cx_i + d)\,\Delta x}{h^2} \sum_{j=1}^{N} x_{ij} K'_{ij}.$$

The first term vanishes as before and since K'_{ij} is odd and x_{ij}^2 is even the second term also vanishes to yield

$$(2cx_i + d) \approx -(2cx_i + d)\frac{\Delta x}{h^2} \sum_{j=1}^{N} (x_i - x_j) K'_{ij}.$$

Thus using the same substitutions as before,

$$1 \approx -2 \sum_{l=1}^{\infty} l \left(\frac{\Delta x}{h}\right)^2 K'\left(l \frac{\Delta x}{h}\right).$$

This shows that the same equation that guarantees exact equality for linear functions also guarantees exact equality for quadratic functions. However, this relationship does not seem to hold exactly for even higher order polynomials.

Therefore, no matter what kernel is selected it will not satisfy Eq. (8) for some (probably most) values of $\Delta x/h$. By choosing a particular $\Delta x/h$, it is possible to find which kernels satisfy the equation or vice versa. This is very useful in selecting the initial particle separation for a given kernel. But this one point does not provide a sufficient indication of what happens after the particles move. However, if an interval of $\Delta x/h$ values is studied, the quality of the kernel as particles move can be inferred. Of course, this is not exactly the same as in an actual calculation since when particles move the uniform spacing is lost. However, we will verify the results for calculations later in this section.

It should be noted that Meglicki [9] derived a similar result to Eq. (8) for smoothed particle magnetohydrodynamics using a completely different method.

3.1. Result 1: Plots of Merit Equation

The first result is a set of plots from which qualitative results may be obtained. For each kernel, plot

TABLE III

Relative Error Norms for Kernel Result 2

No.	Name	Type	M_1	M_2
1	W_4 B-spline	B	0.0128797	0.0201059
2	Cosine	B	0.0284004	0.0451499
3	$\kappa - 2$ Gaussian	B	0.0901453	0.16566
4	L Gaussian	B	0.0604716	0.0843238
5	Q Gaussian	B	0.0119989	0.0192021
6	T Gaussian	B	0.0320381	0.0405489
7	Quartic-1	B	0.0196585	0.0305967
8	Quartic-2	B	0.0887839	0.125373
9	$\kappa - 2$ Exponential	H	0.512015	0.569665
10	1/X,2	H	0.12708	0.156575
11	1/X,4	H	0.103547	0.130743
12	1/X,10	H	0.0893328	0.115851
13	$-X^2$	H	0.0802408	0.107258
14	$-x - e^{-x}$	P	0.24071	0.293757
15	$4 - X^2$	P	0.291355	0.356247
16	$8 - X^3$	P	0.383839	0.471477
17	Double B-spline	D	0.174244	0.335343
18	Double Q Gauss	D	0.135502	0.219316
19	Double T Gauss	D	0.274792	0.343851
20	Double Q-1	D	0.193422	0.289148

$$f_1\left(\frac{\Delta x}{h}\right) = -2\sum_{l=1}^{\infty} l\left(\frac{\Delta x}{h}\right)^2 K'\left(l\frac{\Delta x}{h}\right)$$

$$f_2\left(\frac{\Delta x}{h}\right) = 1.$$

Four such plots for the range $(\Delta x/h) \in [0.1, 2.0]$ are shown in Fig. 2. Note: for kernels that are undefined at $K'(0)$, such as hyperbolic, we assign the average value of 0 ($K'(0) = 0$) and continue with the analysis.

Although the plot for each kernel function is unique, the four shown in Fig. 2 are fairly representative of their respective shape categories. From these plots three observations may be made: First, an overall opinion as to which kernels are better than others. We are looking for how close f_1 is to 1 and when it is not, how far from 1 does f_1 migrate. Second, a list of approximate values where each kernel provides exact results can be obtained. These are good initial particle separation values and can be found precisely using a math program such as Mathematica or MathCAD. Third, a better understanding as to what happens when the particle separation becomes too large. For almost every kernel, the results start becoming quite poor when $\Delta x = h$. Of course, for most of the kernels, the results are completely wrong when the separation approaches κh since nothing is being averaged there. It was shown by Swegle *et al.* [10] and Fulk [2] that there are stability problems with SPH in tension. Tension, of course, tends to force particles apart, so the tension instability is worsened by the fact that the SPH approximation becomes very poor when particles are too sparsely spaced. This result points out that the instability and inaccuracy can get intermixed, so that it may be difficult to determine which is the root of a particular problem.

3.2. Result 2: Error Norms

Although the output of Result 1 provides good qualitative results, it is desirable to obtain quantitative results as well. To do this, perform relative error norms based on Eq. (8). In this subsection both l_1 and l_2 relative error norms are calculated for 100 values of $(\Delta x/h) \in [0.2, 1.2]$. These are labeled as M_1 and M_2 as they are the proposed measures of merit for the quality of a kernel. The formulas for these are

$$M_1 = \left(\frac{1}{100}\right)\sum_{n=1}^{100}\left|-2\sum_{l=1}^{\infty} l\left(0.2+\frac{n}{100}\right)^2 K'\left(1\left(0.2+\frac{n}{100}\right)\right)-1\right| \tag{9}$$

$$M_2 = \sqrt{\left(\frac{1}{100}\right)\sum_{n=1}^{100}\left[-2\sum_{l=1}^{\infty} l\left(0.2+\frac{n}{100}\right)^2 K'\left(l\left(0.2+\frac{n}{100}\right)\right)-1\right]^2}. \tag{10}$$

l_∞ norms can also be calculated, but they are easily inferred from the previous plots. The interval [0.2, 1.2] can be argued as being arbitrary. However, it was chosen as follows:

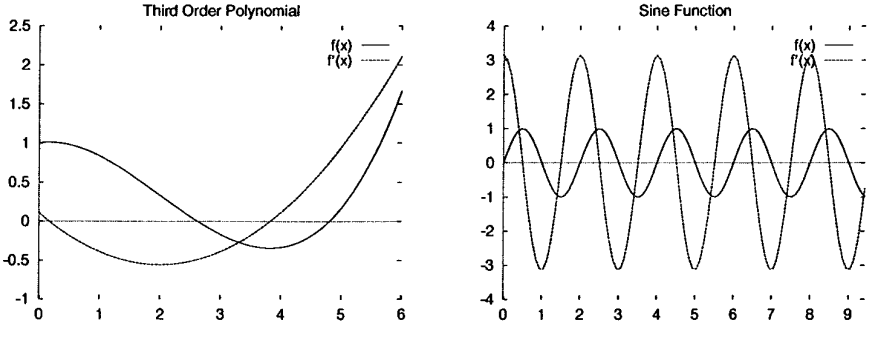

FIG. 3. Verification test functions.

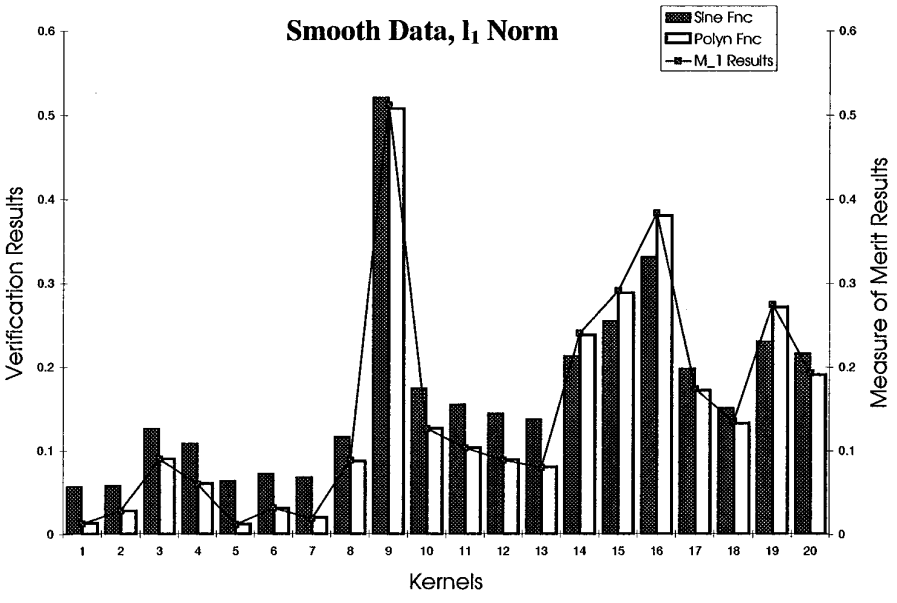

FIG. 4. Bar chart for verification l_1 data.

all of the kernels are very accurate for sufficiently small values of $\Delta x/h$, but seldom does one have the computer resources to compute with that many particles. Also, all of the kernels perform poorly when the values become too large, and that might improperly skew the measure of merit. So a reasonable range was set. Further, the range was centered on 0.7 (a popular value) and was chosen large enough to apply to fixed h problems. The ratio $\Delta x/h$ is more likely to vary over a wider range in a calculation using fixed h than one using variable h. If for a particular problem more information is available on the ranges of Δx, h, or the ratio of the two other more appropriate intervals can be easily used. Other information can come from the physical process being modeled. We encourage readers to modify the range of $\Delta x/h$ in Eqs. (9) and (10) for their particular problems. The results for the 20 kernels being studied here are shown in Table III.

A few general comments can be made regarding the

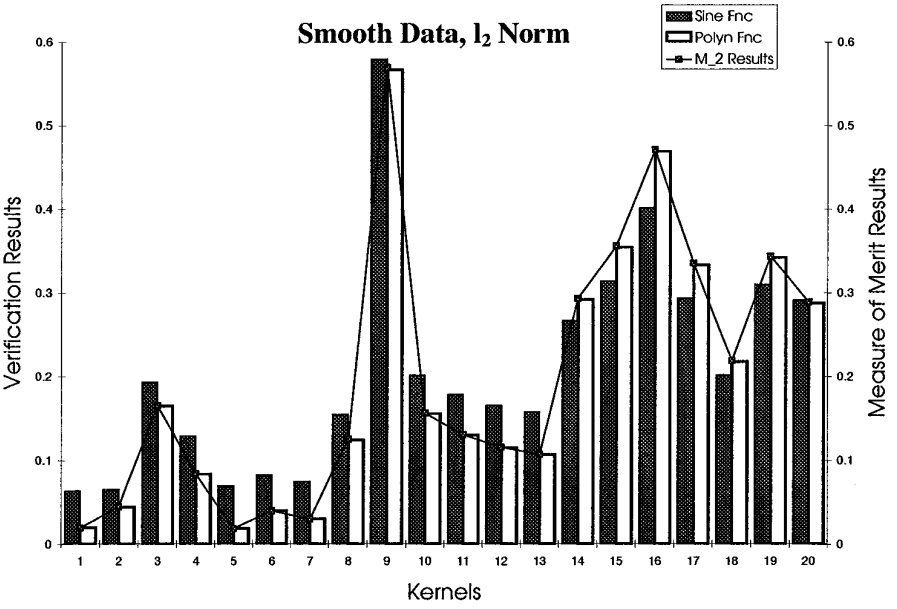

FIG. 5. Bar chart for verification l_2 data.

TABLE IV

Initial Particle Spacing for Calculations

No.	Name	Type	$\Delta x/h$	nph
1	W_4 B-spline	B	0.689898	1.44949
2	Cosine	B	0.673815	1.484087
3	$\kappa - 2$ Gaussian	B	0.666667	1.5
4	L Gaussian	B	0.666667	1.5
5	Q Gaussian	B	0.739626	1.352035
6	T Gaussian	B	0.769779	1.299073
7	Quartic-1	B	0.685996	1.457735
8	Quartic-2	B	0.733263	1.363767
9	$\kappa - 2$ Exponential	H	0.666667	1.5
10	1/X,2	H	0.757363	1.320144
11	1/X,4	H	0.777197	1.286486
12	1/X,10	H	0.791098	1.264131
13	$-X^2$	H	0.799783	1.250274
14	$-x - e^{-x}$	P	0.807503	1.238386
15	$4 - X^2$	P	0.81096	1.233106
16	$8 - X^3$	P	0.816495	1.224747
17	Double B-spline	B	0.698011	1.432642
18	Double Q Gauss	B	0.751723	1.330277
19	Double T Gauss	B	0.787407	1.269991
20	Double Q1	B	0.688891	1.451608
21	Gaussian	B	1.00316	.996849
22	Exponential	H	3.0	0.333333
23	Super Gaussian	B	1.0	1.00
24	Enhanced B-spl	B	0.753059	1.327917

data in Table III. First, the six best kernels are all bell shaped (B), the next six are either bell (B) or hyperbolic (H) shaped. The parabolic (P) and double hump (D) shaped kernels performed the poorest. We expected the double humped kernels to perform better than they did. However, after further investigation, since they have a shape that changes more often, more particles are required to accurately reflect those changes. Since the number of particles was the same for all kernels, they do not perform as well. Second, although some shapes are in general better and others poorer, vigilance is required in selecting a kernel. Third, these measures of merit are macro-measures. That is, they are useful in identifying groupings of better and poorer kernels, but care must be given not to try and use a measure of merit to decide among the kernels of any one of the groupings.

3.3. Verification

Although Results 1 and 2 have a theoretical basis, they are only guaranteed to show a kernel's worth for polynomial functions up to quadratic. However, we propose the measures of merit shown under Result 2 can be used for any function. If h is small enough (and Δx also small) this is certainly true (any smooth function is nearly linear if a small enough interval in considered). To support this proposal, we use two verification tests: first, a static test of the SPH derivative; second, a test using actual SPH calculations.

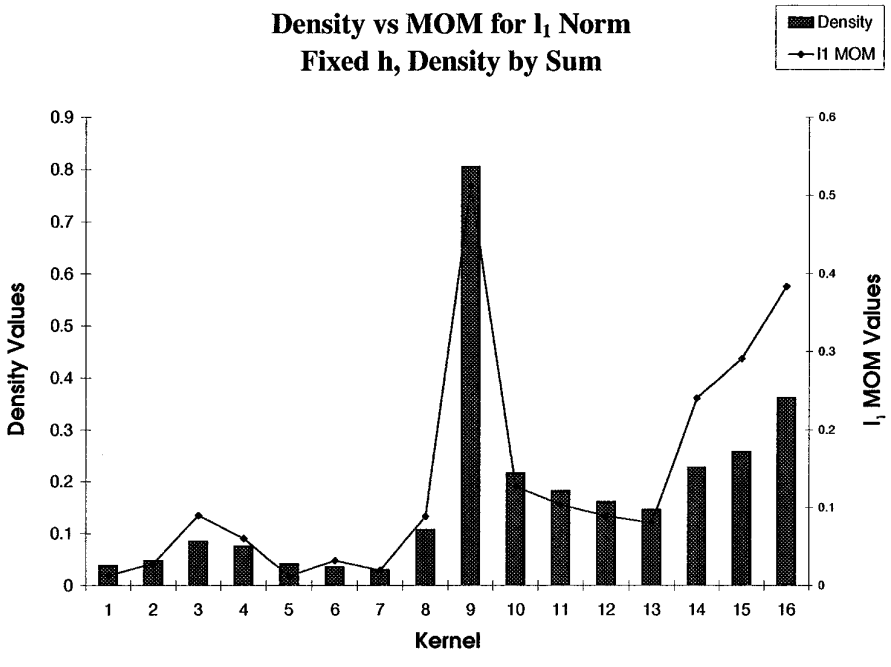

FIG. 6. Riemann shock tube, fixed h, density, l_1 data.

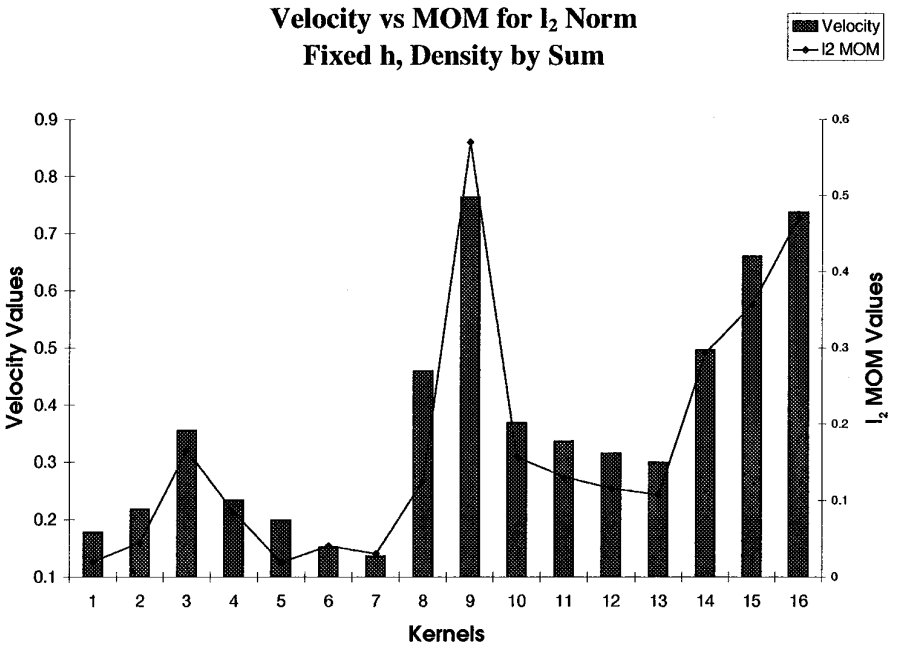

FIG. 7. Riemann shock tube, fixed h, velocity, l_2 data.

3.3.1. *Static Verification*

To verify the measures of merit given in Eqs. (9) and (10) apply to other more general functions, two test functions are used. These are

- a third order polynomial: $(x^3 - 6x^2 + 2x + 18)/18$ on $[0, 6]$;
- a sine function: $\sin(\pi x)$ on $[0, 3\pi]$

Plots of these two functions and their corresponding derivatives are shown in Fig. 3. l_1 and l_2, relative error norms, are calculated for a given $\Delta x/h$ as follows: f is the function to be evaluated and S is the SPH approximation to f',

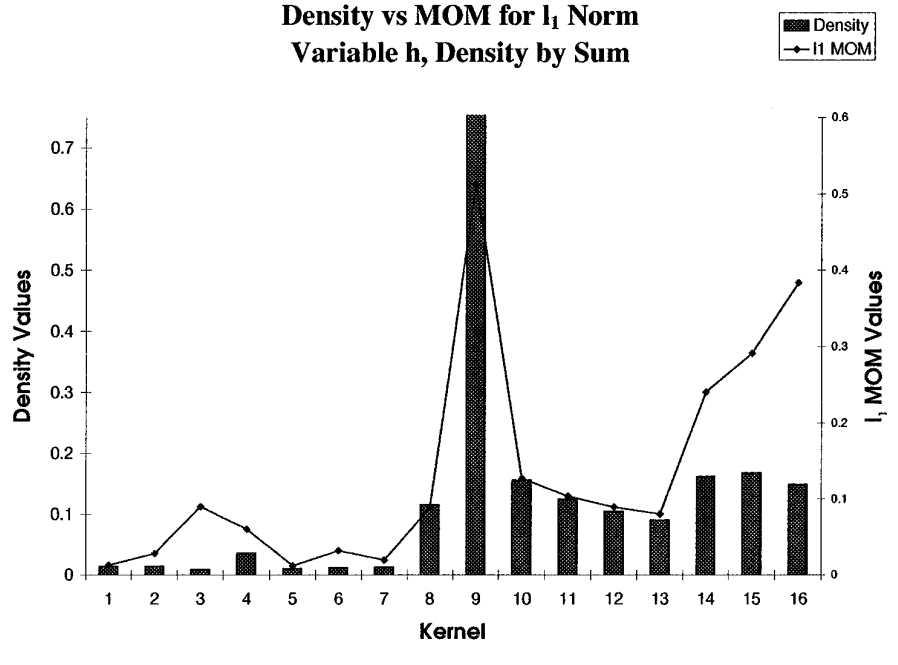

FIG. 8. Riemann shock tube, variable h, density, l_1 data.

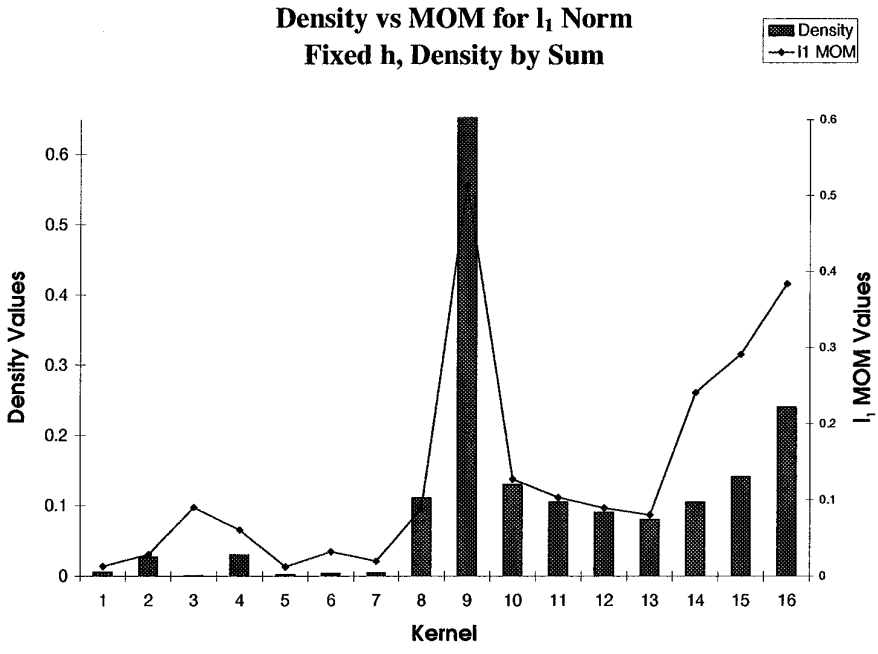

FIG. 9. HSTC, fixed h, density, l_1 data.

$$l_1\left(\frac{\Delta x}{h}\right)=\frac{\sum_{i=0}^{N}|f'(x_i)-S(x_i)|}{\sum_{i=0}^{N}|f'(x_i)|}$$

$$l_2\left(\frac{\Delta x}{h}\right)=\frac{\sqrt{\sum_{i=0}^{N}(f'(x_i)-S(x_i))^2}}{\sqrt{\sum_{i=0}^{N}(f'(x_i))^2}},$$

where $N = (x_{\max} - x_o)/\Delta x$ and $x_i = x_o + i\,\Delta x$. For the cubic, $[x_o, x_{\max}] = [0, 6]$ and for the sine function, $[x_o, x_{\max}] = [0, 3\pi]$. To obtain a single number for each kernel, 100 values of $\Delta x/h$ are used to calculate an average (absolute or square) of the l_1 and l_2 errors described above. The ranges chosen are $h \in [0.1, 0.2]$ and $\Delta x \in [0.02, 0.24]$, implying $\Delta x/h \in [0.2, 1.2]$ (the same as for the measures of merit). The formulas for these are

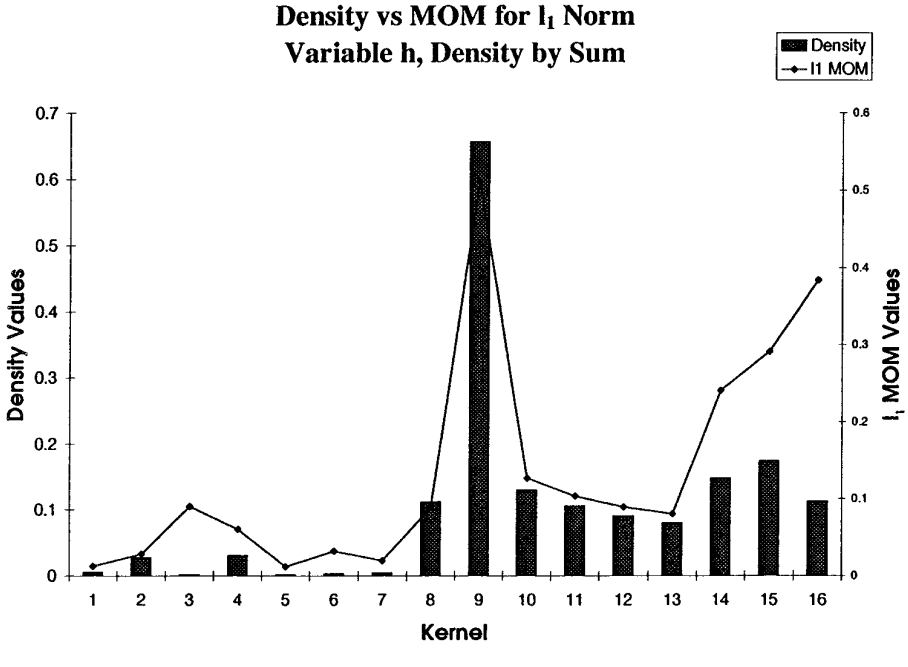

FIG. 10. HSTC, variable h, density, l_1 data.

TABLE V

Additional Kernels

Name	$\mathscr{K}(u)$	κ	1D c_n
Gaussian	e^{-u^2}	3	$\frac{1}{\sqrt{\pi}}$
Exponential	$e^{-\lvert u\rvert} - e^{-9}$	9	0.500618
Super-Gaussian	$\left(\frac{3}{2} - u^2\right) e^{-u^2}$	3	$\frac{1}{\pi^{1/2}}$
Enhanced B-spline	$\begin{cases} 17 - \frac{147}{4}u^2 + \frac{18}{4}\lvert u\rvert^3 & \text{if } 0 \le \lvert u\rvert \le 1 \\ \frac{1}{4}(2 - \lvert u\rvert)^2(49 - 47\lvert u\rvert) & \text{if } 1 \le \lvert u\rvert \le 2 \end{cases}$	2	$\frac{1}{18}$

$$\langle l_1\rangle = \sum_{n=0}^{100}\left(\frac{1}{101}\right)\left|l_1\left(0.2 + \frac{n}{100}\right)\right| \tag{11}$$

$$\langle l_2\rangle = \sqrt{\sum_{n=0}^{100}\left(\frac{1}{101}\right)\left[l_2\left(0.2 + \frac{n}{100}\right)\right]^2}. \tag{12}$$

The results are displayed as bar charts shown in Figs. 4 and 5. In these figures, the line with small boxes is the predicted goodness from the measure of merit (Eqs. (9) and (10)) and the bars are for the functions described in Eqs. (11) and (12).

Some general conclusions can be drawn from these figures for smooth data. First, the Result 2 measure of merit (norms given in Table III) very closely match the norms from the test functions. This implies that the error norm from Result 2 is a good measure of merit of a kernel (at least globally) for smooth data. Second, since the data match Result 2 so well, the same conclusions made earlier that bell shaped kernels are better still applies.

3.3.2. *Actual Calculation Verification*

To further verify the measures of merit given in equations (9) and (10) apply to actual calculations, two test cases are used. They are both performed using standard SPH equations applied to the equations of gas dynamics (see Monaghan [1]). These are

- Hydrodynamic smooth test case (HSTC). This test has velocity constant everywhere and density constant except for a Gaussian shaped perturbation in a small area. Energy is set to $1/\rho$ which makes pressure constant everywhere under the ideal gas law equation of state. The analytic solution to this problem after a given time has all the field values the same as the initial conditions, simply moved to the right (or left) by velocity*time.
- Riemann shock tube. This is a classic test case described in several places, including Sod [11] and Monaghan and Gingold [12]. The density ratio for this test case was 8:1. Although in some respects this is a shock test and not a smooth data test, once artificial viscosity is added, discontinuities are smoothed and the results of this section should apply.

TABLE VI

Relative Error Norms for Additional Kernels Result 2

Name	Type	M_1	M_2
Gaussian	B	0.00279564	0.00621844
Exponential	H	0.0463731	0.0565237
Super-Gaussian	B	0.0191325	0.0429511
Enhanced B-spline	B	0.0882854	0.129977

The initial particle spacing was chosen for each kernel as shown in Table IV. These values were calculated so that the error from Result 1 or 2 is zero and so that there are four particles within the support for any kernel.

The tests for each kernel were performed for both fixed and variable h configurations. Density was calculated using the summation form due to difficulties using the continuity equation for these test cases. l_1 and l_2 relative error norms are calculated for density, energy, velocity, and pressure for each problem. Selected plots are shown in Figs. 6–10. These represent a cross section of l_1 vs l_2 norms, field variables, and fixed vs variable h. As expected the results match the measure of merit better for fixed h since the measure of merit was based on a large range of $\Delta x/h$ values.

We note that kernels 17–20 are not shown in the test cases. These are all the double-hump kernels. We had difficulty getting these implemented in SPH so that the test cases would run to completion. There could be several

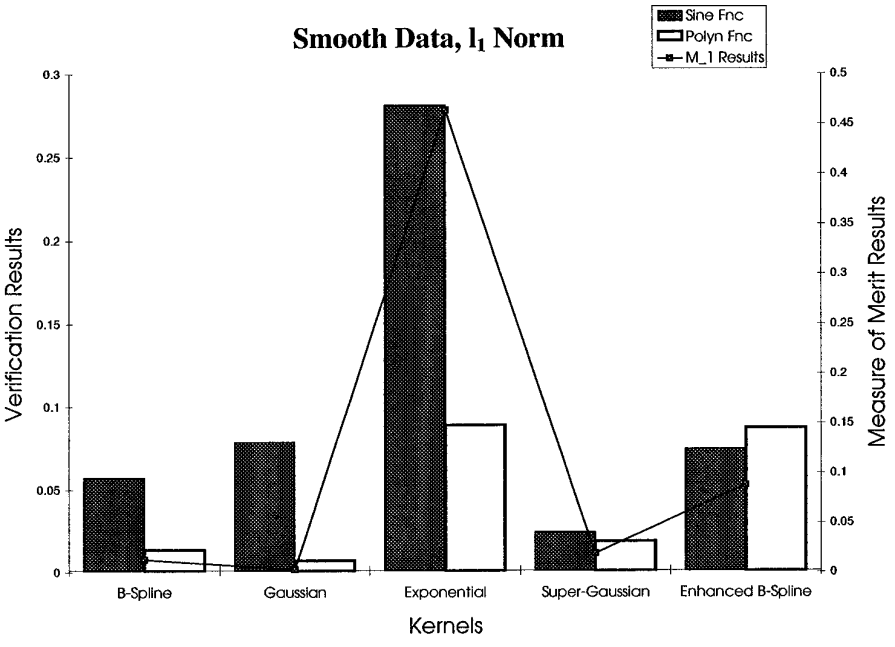

FIG. 11. Bar chart for verification, l_1, smooth data, additional kernels.

reasons for this. However, it is our feeling that for general problems, especially with rather sparse spacing of particles, these will not prove to work very well.

Some general conclusions can be drawn from these figures. First, the Result 2 measure of merit (norms given by Eqs. (9) and (10) and in Table III) very closely match the norms from the test cases. This implies that the error norm from Result 2 is a good measure of merit of a kernel (at least globally) for actual calculations. These tests validate our contention that these measures of merit are not simply theoretical curiosities, but useful predictors of a kernel's relative worth. Second, since the data match Result 2 so

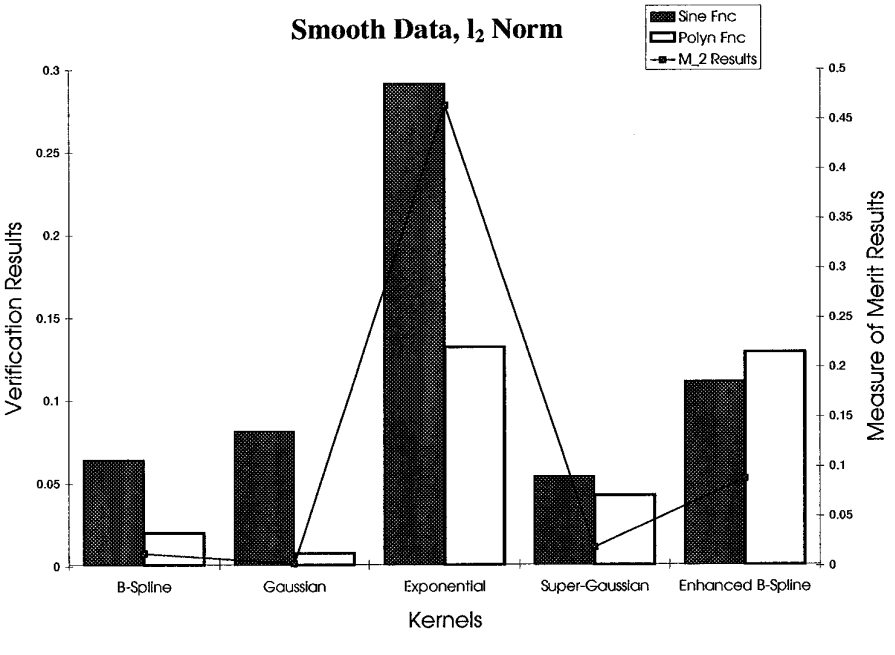

FIG. 12. Bar chart for verification, l_2, smooth data, additional kernels.

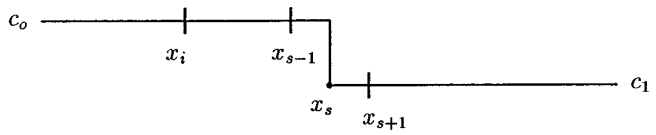

FIG. 13. Non-smooth data example.

well, the same conclusions made earlier that bell shaped kernels are better still applies. Several of the bell shaped kernels performed quite well and, based on this measure of merit, we would rate them all roughly equivalent.

4. OTHER COMPARISONS

Up until now, only *standard* second-order SPH kernels were evaluated and compared in this paper. However, other kernels such as kernels with support greater than 2 and higher order kernels also can be considered. There are only a few kernels in the published literature with support greater than 2. This is because they add extra smoothing (average across more particles) and are less efficient than using other forms. However, for completeness we present two of these kernels, the Gaussian and the exponential. Although neither of these functions actually has compact support, they are treated as zero outside of $3h$ and $9h$, respectively. The other kernels considered here are known as higher order kernels. They satisfy

$$0 = \int_\Omega u^2 W(-u, h)\, du.$$

Since the kernel is assumed to be even, the next term in the error analysis (involving u^3) will vanish leaving the error term proportional to an integral involving u^4. Of course, even higher order kernels can be developed if desired. The two considered here are the enhanced B-spline and the super-Gaussian. All four kernels are shown in Table V.

Since the analysis performed in this paper so far did not rely on the value of κ (the support) or the order, comparisons between these kernels and those previously studied is easily accomplished.

First, the integral test (from Section 2) will result in 0 for the higher order kernels, since that is the definition of being higher order. This implies, when compared with the results in Table II, the higher order kernels should perform better. However, as previously noted, the integral test is only relevant when $\Delta x/h$ is sufficiently small. Also, the integral test for the Gaussian and exponential produces values of 0.24989 and 0.979983, respectively. Since these kernels are spread over a wider range (in some sense less peaked), we would not expect them to perform as well as the others and, indeed, they are poorer with respect to the results in Table II.

Second, the Result 2 norms of Section 3.2 for these four kernels are given in Table VI. As compared with standard kernels found in Table III, the Gaussian performs quite well and the exponential slightly better than other hyperbolic shaped kernels (and even better than some bell shaped). The results for the higher order kernels are initially somewhat surprising. The results are at best average for their shaped category (bell shaped). Although the results do not make these poorer kernels to use, they do not have any advantages over more standard, lower order kernels. There are two reasons for this. First, since only the kernel approximation is made better by a higher order kernel, the number of particles must be significantly increased before the errors in the particle approximation are of the same order as the kernel approximation (Δx must approach h^3). Second, the higher order kernels have more elaborate shapes than standard kernels (including regions where they are negative). But unless enough particles are used to take advantage of that shape, it just adds more noise.

TABLE VII

Kernel Value at 0

No.	Name	Type	$K(0)$	S_1	S_2
1	W_4 B-spline	B	0.666667	0.533333	0.355556
2	Cosine	B	0.575169	0.597382	0.343595
3	$\kappa - 2$ Gaussian	B	0.846553	0.407413	0.344897
4	L Gaussian	B	0.785348	0.450256	0.353608
5	Q Gaussian	B	0.643998	0.549201	0.353685
6	T Gaussian	B	0.580569	0.593602	0.344627
7	Quartic-1	B	0.625	0.5625	0.351563
8	Quartic-2	B	0.416667	0.708333	0.295139
9	$\kappa - 2$ Exponential	H	2.250277	−0.575194	−1.294346
10	1/X,2	H	0.917133	0.358007	0.328340
11	1/X,4	H	0.837880	0.413484	0.346450
12	1/X,10	H	0.78646	0.449478	0.353496
13	$-X^2$	H	0.75	0.475	0.35625
14	$-x - e^{-x}$	P	0.403745	0.717379	0.289638
15	$4 - X^2$	P	0.375	0.7375	0.276563
16	$8 - X^3$	P	0.33333	0.766667	0.255556
17	Double B-spline	D	0.0	1.0	0.0
18	Double Q Gauss	D	0.0	1.0	0.0
19	Double T Gauss	D	0.0	1.0	0.0
20	Double Q-1	D	0.0	1.0	0.0

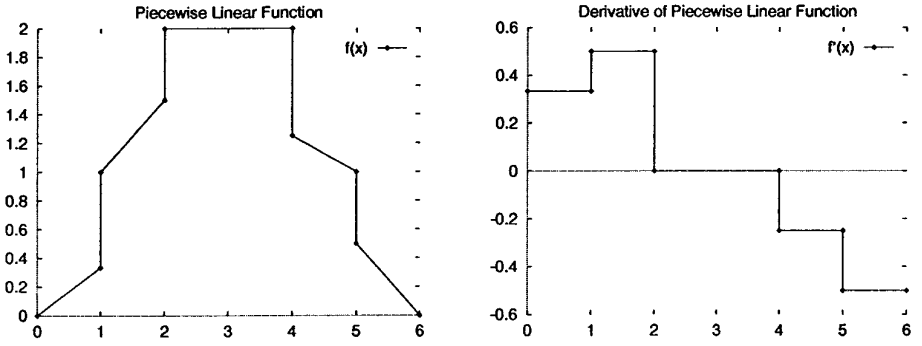

FIG. 14. Verification test functions for non-smooth data.

Last, the static verification results, corresponding to the test functions described in the previous section are again shown in bar chart form in Figs. 11 and 12. The W_4 B-spline kernel (No. 1) is included for comparison with one of the better standard kernels.

Since the Result 2 norms represent the verification results fairly well, the conclusions are the same. The Gaussian kernel can be considered as one of the better kernels, but at a cost of more computation time. Overall, the higher order kernels do not gain very much, if anything. They have regions where they are negative and drop off fast when sparsely spaced. The primary gain would be realized if the number of particles per h was quite large ($\Delta x/h$ quite small).

5. NON-SMOOTH DATA

In this section, the previous work in this paper is extended to areas near a shock (assuming no smoothing such as artificial viscosity). However, the uniform spacing assumptions still remain. Consider Fig. 13 and Eq. (13):

$$f = \begin{cases} c_o & \text{if } x \le x_s \\ c_1 & \text{if } x > x_s. \end{cases} \tag{13}$$

Near the shock,

$$f_i' \approx \sum_{j=1}^{N} \Delta x_j f_j W_{ij}' = \Delta x\, c_o \sum_{j=1}^{s} W_{ij}' + \Delta x\, c_1 \sum_{j=s+1}^{N} W_{ij}'.$$

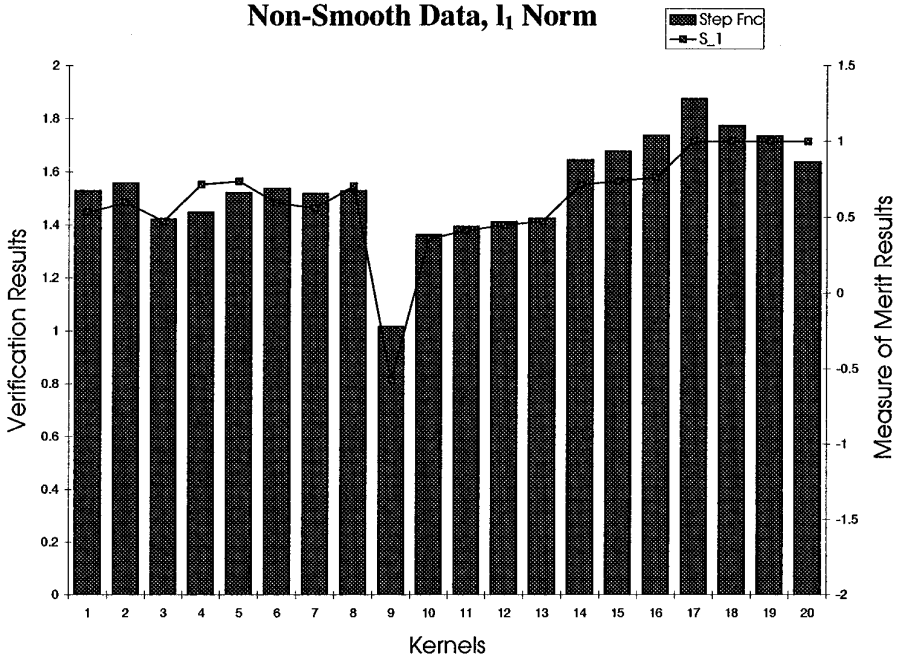

FIG. 15. Bar chart for verification, l_1, non-smooth data.

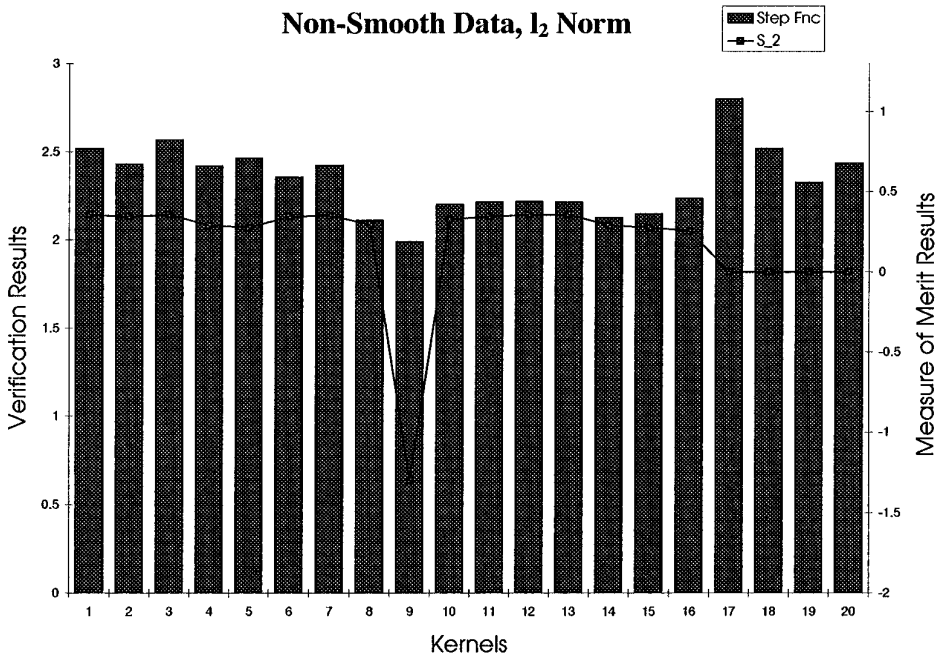

FIG. 16. Bar chart for verification, l_2, non-smooth data.

Let $i < s$. Because W'_{ij} is odd, terms from $i + 1$, ..., s cancel with terms from $2i - s$, ..., $i - 1$, leaving

$$f'_i \approx \Delta x\, c_o \sum_{j=1}^{2i-s-1} W'_{ij} + \Delta x\, c_1 \sum_{j=s+1}^{N} W'_{ij}$$

$$= (c_o - c_1) \sum_{j=1}^{2i-s-1} \Delta x\, W'_{ij}.$$

The sum approximates the right tail area under the W' curve. As $i \to s$ the sum approximates more of the tail, approaching the area under the entire right half of the W' curve. Note: $i > s$ just results in the opposite (left) side of the curve. Thus f'_i approximately equals

$$f'_i \approx (c_o - c_1) \sum_{j=1}^{2i-s-1} \Delta x\, W'_{ij} \approx (c_o - c_1) \int_{x_1}^{x_i-(x_s-x_i)} W'(x_i - \xi)\, d\xi$$

$$= (c_o - c_1) \int_{x_i-x_1}^{x_s-x_i} W'(u)(-du) = (c_o - c_1) \int_{x_s-x_i}^{\kappa h} W'(u)\, du$$

$$= (c_o - c_1)[W(\kappa h) - W(x_s - x_i)].$$

By the continuity and compact support properties of the kernel, f'_i is approximately equal to $(c_0 - c_1)W_{si}$. Since the actual value of f'_{s-} is 0, an estimate of the l_1 error norm is

$$\sum_{i=1}^{N} \Delta x_i\, |f'_i| \approx |c_o - c_1| \sum_{i \neq s} \Delta x_i\, W_{is}$$

$$= |c_o - c_1| \left[\sum_{i=1}^{N} \Delta x_i\, W_{is} - \Delta x\, W_o \right].$$

The summation term at the end of the last equation is an approximation of the integral of W, which is just 1. Since c_o and c_1 are arbitrary and independent of the choice of the kernel, the following is proposed as a measure of merit for kernels using the l_1 norm for non-smooth data (S_1):

$$\min(1 - \Delta x\, W_o) = \min\left(1 - \frac{\Delta x}{h} K_o\right). \tag{14}$$

The same steps can be performed to arrive at the following as a measure of merit for kernels under the l_2 norm for non-smooth data (S_2):

$$\min[W_o(1 - \Delta x\, W_o)] = \min\left[\frac{1}{h} K_o \left(1 - \frac{\Delta x}{h} K_o\right)\right]. \tag{15}$$

The values of $K(0)$, $S_1 = 1 - 0.7 * K(0)$, and $S_2 = K(0) * (1 - 0.7 * K(0))$ for the 20 kernels are shown in Table VII. Note: 0.7 is used since it is an average value for $\Delta x/h$ in this study.

The data in Table VII show that the results are somewhat

different under an l_1 norm than an l_2 norm. For the l_1 norm, based on the column S_1, the hyperbolic shapes (H) perform the best while the parabolic shapes (P) perform the worst. It should be noted that many of the numbers are quite close, but not as close as for the l_2 norm. From the last column in the table, almost all kernels delivered similar results for the l_2 norm. The parabolic shapes are slightly better (with one exception for kernel 9), but the rest are then roughly the same.

These ideas will now be verified against a test function. Since these results are for non-smooth data, a step function was chosen such that it is linear with several jump discontinuities. The function and its derivative is shown in Fig. 14.

The step function is then used as before to verify the results by calculating l_1 and l_2 norm errors. These results and the non-smooth measures of merit are shown in the bar charts shown in Figs. 15 and 16. The lines with small boxes represent the information above and the bars are from the verification function.

Some general conclusions may be drawn from these figures. First, the S_1 and S_2 measures of merit (data given in Table VII) match the norms from the test function fairly well. The match is not as good as for smooth data, indicating it may need some minor modifications. Second, based on the measure of merit and data in the figures there does not appear to be any class of kernels that are significantly better than the others under both norms for non-smooth data. The $\kappa - 2$ exponential has the least error. However, due to the shape of this kernel (very sharply peaked) it may not be a very good choice.

6. SUMMARY

This paper provides two primary results in addition to several smaller items. First, a measure of merit for SPH kernels is derived. Although it is used here for a specific interval of values of $\Delta x/h$, the technique is valid for any interval a user wishes to apply. Through a static validation test and the theory developed here, it can be concluded that the key variables in a kernel's worth is the shape and the value of $\Delta x/h$. This measure of merit provides an objective method based on problem information of determining a set of kernels that should provide better results. Second, 20 kernels are analyzed showing the tendency for bell shaped kernels to outperform other shapes for SPH in regions of smooth data. These results are validated using a hydrodynamic smooth test case and the classic Riemann shock tube test case. Some of the lessor results are for higher order kernels and kernels near discontinuities. For the choices of Δx and h which lead to efficient calculations for the standard kernels, the higher order kernels (super Gaussian and enhanced B-spline) are shown not to be significantly better than the standard order kernels. Also, it was shown that near discontinuities, the shape of the kernel is no longer a prime factor in determining accuracy.

The authors are continuing this research to determine if the analysis here in one dimension carries over to higher dimensions. Initial results indicate that kernels follow a very similar pattern in higher dimensions as in one dimension. Additional future work might include new kernels that reduce the errors shown here and paramaterizing bell shaped kernels to reduce the error. Also new variable smoothing length formulations that restrict the growth of $\Delta x/h$ to ensure that kernel spacing does not cause inaccuracies should be considered.

REFERENCES

1. J. J. Monaghan, *Annu. Rev. Astronom. Astrophys.*, **30,** 543 (1992).
2. D. A. Fulk, Ph.D. dissertation, Department of Mathematics and Statistics, Air Force Institute of Technology, Wright-Patterson AFB, OH, 1994 (unpublished).
3. D. A. Fulk and D. W. Quinn, in revision.
4. J. J. Monaghan, *J. Comput. Phys.* **110,** 399 (1994).
5. L. D. Libersky, A. G. Petschek, T. C. Carney, J. R. Hipp, and F. A. Allahdadi, *J. Comput. Phys.* **109,** 67 (1993).
6. D. Wood, *Mon. Not. R. Astronom. Soc.* **194,** 201 (1981).
7. J. J. Monaghan, *J. Comput. Phys.* **60,** 253 (1985).
8. J. P. A. Morris, Monash University paper, Clayton, Victoria, Australia, 1993 (unpublished).
9. Z. Meglicki, *Comput. Phys. Commun.* **81,** 91 (1994).
10. J. W. Swegle, S. W. Attaway, M. W. Heinstein, F. J. Mello, and D. L. Hicks, Sandia National Laboratory Technical Report SAND93-2513, 1994 (unpublished).
11. G. A. Sod, *J. Comput. Phys.* **27,** 1 (1978).
12. J. J. Monaghan and R. A. Gingold, *J. Comput. Phys.* **52,** 374 (1983).